All-Optical Vector Atomic Magnetometer

B. Patton*
Department of Physics, University of California, Berkeley, California 94720-7300, USA and Physik-Department, Technische Universität München, 85748 Garching, Germany

E. Zhivun
Department of Physics, University of California, Berkeley, California 94720-7300, USA

D. C. Hovde
Southwest Sciences Ohio Operations, Cincinnati, Ohio 45244, USA

D. Budker
Department of Physics, University of California, Berkeley, California 94720-7300, USA
Nuclear Science Division, Lawrence Berkeley National Laboratory, Berkeley, California 94720, USA and Helmholtz Institute, Johannes Gutenberg University, 55099 Mainz, Germany

(Received 28 March 2014; revised manuscript received 23 May 2014; published 1 July 2014)

We demonstrate an all-optical magnetometer capable of measuring the magnitude and direction of a magnetic field using nonlinear magneto-optical rotation in cesium vapor. Vector capability is added by effective modulation of the field along orthogonal axes and subsequent demodulation of the magnetic-resonance frequency. This modulation is provided by the ac Stark shift induced by circularly polarized laser beams. The sensor exhibits a demonstrated rms noise floor of ~65 fT/$\sqrt{\text{Hz}}$ in measurement of the field magnitude and 0.5 mrad/$\sqrt{\text{Hz}}$ in the field direction; elimination of technical noise would improve these sensitivities to 12 fT/$\sqrt{\text{Hz}}$ and 10 μrad/$\sqrt{\text{Hz}}$, respectively. Applications for this all-optical vector magnetometer would include magnetically sensitive fundamental physics experiments, such as the search for a permanent electric dipole moment of the neutron.

DOI: 10.1103/PhysRevLett.113.013001 PACS numbers: 32.60.+i, 07.55.Ge, 11.30.Er, 94.80.+g

Spin-precession magnetometers [1,2] have found widespread application in disciplines ranging from geophysics [3] to medicine [4,5] and fundamental physics [6,7]. Alkali-vapor magnetometers in particular have experienced great advances in recent years, with sensitivities at or below the fT/$\sqrt{\text{Hz}}$ level demonstrated in the laboratory [3,8–10]. Because these devices measure the Larmor precession frequency of atomic spins, they are intrinsically sensitive to the magnitude of an applied field rather than its projection along a particular direction. This can be advantageous, in that precision of the scalar field measurement is not limited by physical alignment of the sensors, as it is in the case of triaxial flux gates or superconducting quantum interference devices. Nevertheless, in many situations it is desirable to have full knowledge of a field's vector components.

There are several ways to derive vector field information from a scalar magnetometer. In bias-field nulling, calibrated magnetic fields are imposed upon the magnetometer in order to achieve a zero-field magnetic-resonance condition [11–13]. With finite-field sensors using radio frequency coils to drive the resonance (e.g., M_x magnetometers [14]), one may add secondary continuous light beams and measure their modulation to extract vector information [15,16]. It is also possible to detect magnetically sensitive resonances in electromagnetically induced transparency (EIT) schemes; the amplitudes of different EIT resonances can yield information about the relative angle between the laser polarization and the field [17,18]. Synchronously pumped magnetometers employing atomic alignment can provide partial vector information in measurement of the angle between the magnetic field and the polarization axis of the linearly polarized pump beam [19].

Perhaps the simplest way to adapt a scalar magnetometer for vector measurements is to operate it in the finite-field regime (e.g., through synchronous optical pumping [20–22]) and apply time-varying fields to it. By applying orthogonal fields modulated at different frequencies, it is possible to demodulate the magnetic-resonance signal and determine which applied fields add linearly with the ambient field and which add in quadrature with it [23–25]. Although this is effective, there are some situations where this approach is infeasible or undesirable. One example would be the case of remote magnetometry [26,27], where it would be impractical to apply fields to a distant atomic sample. A different limitation appears in certain precision physics applications, such as the search for a neutron electric dipole moment (EDM) [7,28–30]. In such experiments, alkali-vapor magnetometers can reduce systematic error by providing crucial magnetic-field information, but only if these sensors do not themselves produce field contamination.

All-optical alkali-vapor magnetometers are particularly well suited for EDM tests, as they can be designed to produce no significant static or radio frequency fields [31].

Here we demonstrate an all-optical vector magnetic sensor based upon nonlinear magneto-optical rotation in cesium vapor. The effective magnetic field seen by the atoms is modulated by ac Stark shifts ("light shifts") induced by orthogonally propagating laser beams. Since the light shift of a circularly polarized beam is analogous [32] to an effective magnetic field oriented along its propagation direction [33–35], a comparison of the Larmor frequency shifts induced by these beams yields a measurement of the field angle. If technical noise were eliminated, this magnetometer would have 12 fT/$\sqrt{\text{Hz}}$ precision in measurement of the field magnitude and 10 μrad/$\sqrt{\text{Hz}}$ in the field direction.

The experimental setup is shown in Fig. 1. The heart of the sensor is a cylindrical antirelaxation-coated [36] Cs vapor cell, approximately 5 cm diameter and 5 cm in length, with a longitudinal spin relaxation time of 0.7 s. This cell is enclosed within four layers of μ-metal magnetic shielding; measurements were performed at ambient temperature. Coils wound on a frame within the innermost shield allow magnetic fields and gradients to be applied to the cell. The field component oriented along $\hat{z}$ is produced by a current generated by a custom supply which can provide up to 150 mA (Magnicon GmbH). This supply is housed in a temperature-stabilized enclosure and exhibits a relative drift of $\sim 10^{-7}$ over 100 s. A second current supply (Krohn Hite 523) is connected to the coil in the $\hat{y}$ direction, allowing the net field $\mathbf{B}_0$ to be tilted in the $\hat{y}$-$\hat{z}$ plane. The pump beam which drives the magnetic resonance is generated by a distributed feedback (DFB) diode laser that is locked with a dichroic atomic vapor laser lock (DAVLL) [37] to the Cs $D1$ transition at 894 nm. The $\hat{x}$-directed pump is circularly polarized and amplitude modulated with an acousto-optic modulator (AOM) at the ^{133}Cs Larmor frequency ω_L to achieve synchronous optical pumping; the modulation waveform is a square wave with a duty cycle of 5%. A separate linearly polarized probe beam, generated by a DFB laser locked with a DAVLL to the Cs $D2$ transition, traverses the cell in the $\hat{y}$ direction. The probe experiences optical rotation [38] in the polarized Cs sample, modulating its polarization at ω_L. This is detected by a balanced polarimeter with a differential transimpedance amplifier; its output is fed into a digital lock-in amplifier (Stanford Research Systems SR830) whose reference frequency is provided by the local oscillator which drives the pump AOM. The phase of the lock-in amplifier is chosen such that the $X(Y)$ output displays an absorptive (dispersive) Lorentzian as the driving frequency is scanned across the resonance. Directly on resonance, the X output is maximum and the Y output is nulled; small shifts in the magnetic-resonance frequency ω_L cause a linear change in the Y output about zero. With a time-averaged pump power of 2.5 μW and a probe power of 10 μW, the peak optical-rotation signal is 5 mrad and the magnetic-resonance linewidth is 2.9 Hz. The dominant contributions to this linewidth are alkali-alkali spin-exchange broadening and slight power broadening due to the pump and probe beams. The beam powers and optical detunings were chosen to optimize the scalar sensitivity of the magnetometer.

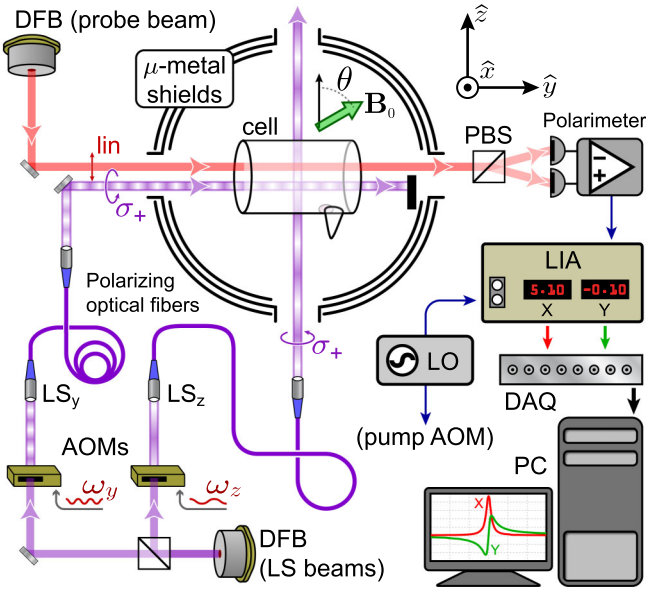

FIG. 1 (color online). Experimental schematic. An amplitude-modulated, circularly polarized pump beam (not shown) propagates in the $\hat{x}$ direction. The local oscillator (LO) controls the pump AOM and serves as a reference to the lock-in amplifier (LIA), whose analog output is recorded by a data acquisition card (DAQ) and read into a computer (PC). A linearly polarized probe beam passes through the cell and is split by the polarizing beam splitter (PBS) of a balanced polarimeter; the output of this polarimeter is demodulated by the lock-in. Two circularly polarized light-shift beams LS_y and LS_z are independently modulated and sent through the cell along $\hat{y}$ and $\hat{z}$. Coils allow the magnetic field $\mathbf{B}_0$ to be tilted in the $\hat{y}$-$\hat{z}$ plane.

In addition to the pump and probe, a third DFB laser tuned near the Cs $D2$ transition can be used to apply light-shift beams LS_y and LS_z in the $\hat{y}$ and $\hat{z}$ directions. The optical frequency of the light-shift laser is actively controlled by using a wavelength meter (Ångstrom/HighFinesse WS-7) and computer control of the laser current. An optimal detuning of $\sim$5 GHz blueshifted from the center of the $F = 4 \rightarrow F' = 5$ $D2$ transition was chosen to allow a large effective magnetic field ($\sim$1 nT/mW) with minimal ($\lesssim$0.5 Hz/mW) broadening of the magnetic-resonance line. This beam is split into two paths, sent through independent AOMs, and then coupled into two polarizing [39] fiber patch cables (Fibercore HB830Z). After the fibers, the light-shift beams are sent through quarter-wave plates to generate circularly polarized beams which pass through the cell along the $\hat{y}$ and $\hat{z}$ axes. Optical pickoffs (not shown in Fig. 1) and photodiodes directly before the shields allow the power of

each light-shift beam to be measured. In an evacuated antirelaxation-coated cell, the alkali atoms rapidly sample the internal volume of the cell and experience a light shift determined by the volume-averaged intensity of the laser beam within the cell. Thus two beams of the same power will possess slightly different light-shift coefficients (measured in nT/mW) when propagating in different directions due to asymmetry of the cell dimensions. Nevertheless, their ratio will remain independent of the optical detuning of the light-shift laser.

To demonstrate the effective magnetic fields produced by LS_y and LS_z, we recorded the data shown in Fig. 2. For this measurement, the primary $\hat{z}$ field was held constant at 946.5 nT and an additional $\hat{y}$ field was varied between -1180.5 and $+1177$ nT. Thus the field's magnitude B_0 changed with its angle θ in the $\hat{y}$-$\hat{z}$ plane, requiring the local oscillator and the lock-in reference phase to be reset for each measurement. Recentering the pump modulation frequency on the magnetic resonance also accounted for the dc shift of $\sim$0.5 nT induced by the static component of the light-shift beams. At each field, the respective light shifts produced by the LS_y and LS_z beams were measured by modulating the two beam intensities at different frequencies (12 and 20 Hz) and demodulating the lock-in Y output in software. The average intensity of each light-shift beam was 0.5 mW. By measuring the effects of the two LS beams simultaneously, the effects of drifting power or optical frequency of the light-shift laser could be mitigated. For reasons discussed in the Supplemental Material [32], the modulation frequencies of the LS_y and LS_z beams were switched several times during each measurement.

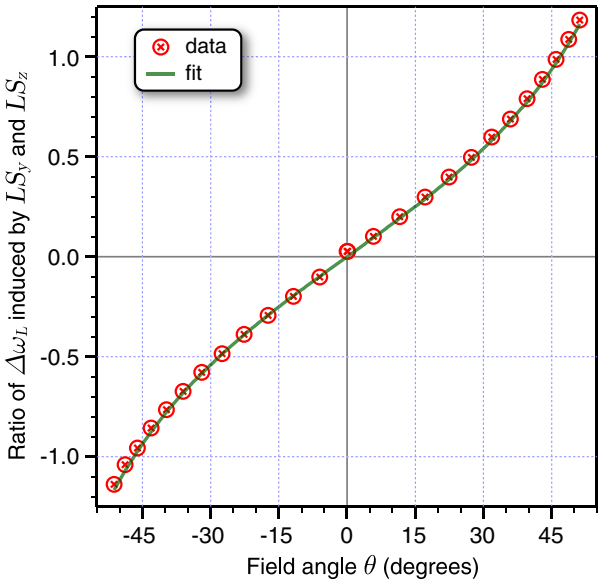

FIG. 2 (color online). The measured ratio of the Larmor frequency shift induced by the LS_y and LS_z beams, plotted as a function of field angle θ from the $\hat{z}$ axis. The curve shows a fit to Eq. (3). Each data point resulted from 20 s of averaging; uncertainties in the data points are below 10^{-2}.

Assume that the magnetometer is operated in the finite-field regime, such that the magnetic-resonance frequency is much higher than the resonance linewidth. The modulated LS_y beam produces an effective magnetic field of magnitude $B_y = P_y\alpha_y[(1/2) + (1/2)\sin(\omega_y t)]$, where P_y is the beam power, α_y is its effective light-shift coefficient, and ω_y is the amplitude-modulation frequency. Similarly, LS_z produces $B_z = P_z\alpha_z[(1/2) + (1/2)\sin(\omega_z t)]$. To maintain the synchronous pumping condition, the fields B_y and B_z are assumed to be comparable to the resonance linewidth (in field units). By adding these fields to the vector components of $\mathbf{B}_0$, the total field magnitude becomes

$$B_{\rm tot} = B_0\sqrt{1 + 2\frac{B_y\sin\theta + B_z\cos\theta}{B_0} + \frac{B_y^2 + B_z^2}{B_0^2}} \approx B_0 + B_y\sin\theta + B_z\cos\theta + \zeta, \quad (1)$$

where the approximation is valid for $B_y, B_z \ll B_0$ and the small quadratic correction ζ is given by

$$\zeta = \frac{(B_y\cos\theta - B_z\sin\theta)^2}{2B_0}. \quad (2)$$

Since the lock-in Y output is proportional to the change in effective Larmor frequency induced by the light-shift fields, demodulation of the signal at frequencies ω_y and ω_z will extract the terms in Eq. (1) proportional to B_y and B_z. Thus the ratio of the measured light shifts is

$$\frac{(\Delta B_{\rm tot})_{LS_y}}{(\Delta B_{\rm tot})_{LS_z}} \approx \frac{P_y\alpha_y}{P_z\alpha_z}\tan\theta. \quad (3)$$

Here we have ignored the contribution from the terms in ζ and other terms of higher power in $(B_{y,z}/B_0)$, which cause modulation of $B_{\rm tot}$ at harmonics other than ω_y and ω_z or scale by powers of $|B_{y,z}/B_0|$ (here $\lesssim 10^{-3}$). We also neglect any effects caused by the tensor light shift, since the circular polarization of the LS beams and their large optical detuning make higher-order light shifts unobservable in the data.

The data shown in Fig. 2 were fit to Eq. (3). The best-fit ratio $(P_y\alpha_y/P_z\alpha_z)$ was measured to be (0.94 ± 0.01) rather than unity, possibly due to slight asymmetry in the cell dimensions or systematic uncertainty of the beam powers within the cell. With no added light-shift beams, the synchronously pumped scalar sensor has a sensitivity of 69 fT/$\sqrt{\rm Hz}$ for measurements at frequencies around 0.5 Hz, as calculated from the linear spectral density (LSD) of the measured magnetic field, shown in Fig. 3. To confirm this sensitivity in the time domain, we stepped the local oscillator frequency by ± 0.875 mHz around ω_L and observed shifts in the lock-in Y output with a

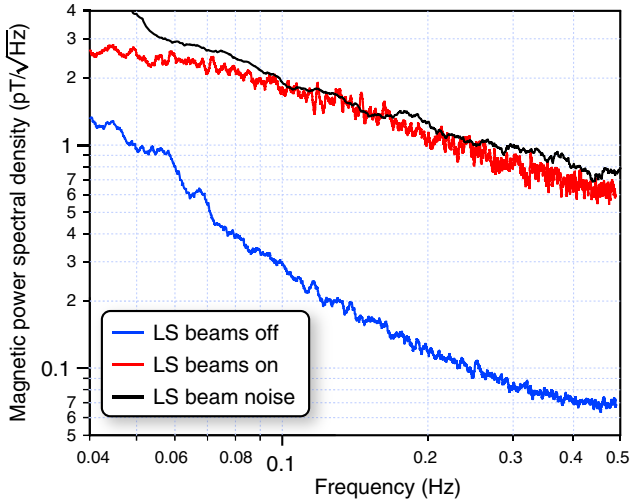

FIG. 3 (color online). Linear-spectral-density plot of the scalar field measurement with the LS_z beams turned off (blue line) and turned on at a constant power of 1 mW (red line). For these data, $\theta = 0$ and the light-shift beam power was not actively controlled. The black trace is the predicted noise floor of the scalar field measurement taken from a (separate) recording of the light-shift beam power, from which a magnetic LSD was derived by using the observed light-shift coefficients α_y and α_z.

signal-to-noise ratio of 7.2. Given the lock-in's equivalent noise bandwidth (ENBW) of 1.25 Hz, this corresponds to a sensitivity of 62 fT/$\sqrt{\text{Hz}}$. To assess the uncertainty in the field angle, we recorded data with the $\hat{z}$ field held constant and the $\hat{y}$ field toggled between two small values. The lock-in Y signal was demodulated at ω_y and ω_z, and the ratio of these two responses converted to a measured magnetic-field angle according to the best-fit curve shown in Fig. 2. The resulting plot of θ vs time is shown in Fig. 4.

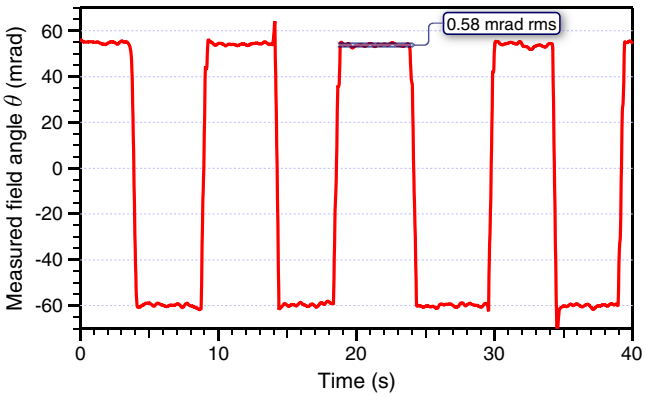

FIG. 4 (color online). Measured field angle θ as a function of time while the applied $\hat{y}$ field is being switched. The average rms noise for a constant field angle translates to a precision of 0.47 mrad/$\sqrt{\text{Hz}}$ in measurement of the field direction. The steps in the plotted ratio are slightly low-pass filtered due to the time constants of the lock-in amplifier and the secondary demodulation at ω_y and ω_z.

The modulation of the field angle is clearly visible, and the rms noise in the ratio corresponds to 0.47 mrad/$\sqrt{\text{Hz}}$ precision in the measured angle of the magnetic field. (This takes into account the measured ENBW of the software demodulation procedure.)

In the present setup, the precision of the measurement of θ is limited by apparent magnetic noise induced by fluctuations in the effective magnetic fields produced by the LS_y and LS_z beams. Such fluctuations arise from instabilities in both the power and the optical detuning of the light-shift laser, although the former effect seems to be dominant in this experiment. With LS_z set to 1 mW without modulation and the field along $\hat{z}$, the smallest observable magnetic-field step with 1 Hz ENBW was 1.3 pT—a factor of 21 worse than the same data recorded without the light-shift beams. Power fluctuations in the LS_y and LS_z beams were recorded and converted into effective magnetic-field fluctuations according to the observed light-shift coefficients $\alpha_{y,z}$. As shown in Fig. 3, the predicted magnetic noise floor matches that observed in the magnetic-field LSD. Better control of intensity noise within the light-shift beams should allow dramatically improved scalar measurements and correspondingly better sensitivity to the field angle. The scalar sensitivity of the magnetometer would be 12 fT/$\sqrt{\text{Hz}}$ if the polarimeter and amplifiers operate at the photon shot-noise limit. By eliminating these sources of technical noise, it should be possible to reach a sensitivity of 10 μrad/$\sqrt{\text{Hz}}$ in the measurement of the magnetic-field direction. This will require stabilization of the LS beam powers to a level of $\sim$10 nW$\sqrt{\text{Hz}}$ and optical frequency stability to the level of $\sim$0.1 MHz$\sqrt{\text{Hz}}$, experimentally realistic goals which are much less stringent than the state of the art [40].

Expanding the vector measurement to three dimensions will simply require adding another light-shift beam in the $\hat{x}$ direction. The bandwidth of the vector measurement is presently limited by the narrow magnetic-resonance line, but this can be extended by power broadening the resonance with the probe beam or heating the cell to increase the Cs density and spin-exchange-broadened linewidth. Either technique would allow more rapid measurement of the vector field components with little if any loss in sensitivity. As discussed in the Supplemental Material [32], the uncertainty in the measured angle θ has no intrinsic dependence on the magnitude of the ambient field B_0. Since magnetometry via synchronous optical pumping has been demonstrated to work in the geophysical field range [1,41], this sensor could be employed for precise vector field measurements at Earth's field with no substantial changes to the experimental apparatus or procedure (apart from the elimination of the μ-metal shields).

In summary, we have demonstrated a method for measuring the magnitude and direction of a magnetic field through all-optical interrogation of an atomic sample. This approach has the advantage that it relies upon measurement

of shifts in the magnetic-resonance frequency, which can be quantified precisely. Further optimization of the apparatus will allow for a compact, magnetically inert vector magnetometer well suited for precision physics experiments or geophysical field measurement. We note that vector light shifts have recently been employed to improve sensitivity by modulating the effective field seen by a chip-scale scalar atomic magnetometer operating at near-zero field [42].

We thank Douglas Beck, Michael Sturm, David Wurm, and Peter Fierlinger for their helpful input, Mikhail Balabas for preparation of the antirelaxation-coated cesium cell, and Arne Wickenbrock for contributions to the measurement. This work was funded in part by a University of California UC Discovery Proof of Concept grant (No. 197073) and NASA SBIR Contract No. NNX13CG20P and is supported by National Science Foundation Grant No. PHY-1068875. B. P. is supported by DFG Priority Program SPP1491, "Precision Measurements with Cold and Ultracold Neutrons."

*Present address: AOSense, Inc., Sunnyvale, CA 94085, USA.
BPattonUCB@gmail.com

[1] D. Budker and D. F. Jackson Kimball, *Optical Magnetometry* (Cambridge University Press, New York, 2013).
[2] D. Budker and M. Romalis, Nat. Phys. **3**, 227 (2007).
[3] H. B. Dang, A. C. Maloof, and M. V. Romalis, Appl. Phys. Lett. **97**, 151110 (2010).
[4] G. Bison, N. Castagna, A. Hofer, P. Knowles, J.-L. Schenker, M. Kasprzak, H. Saudan, and A. Weis, Appl. Phys. Lett. **95**, 173701 (2009).
[5] C. N. Johnson, P. D. D. Schwindt, and M. Weisend, Phys. Med. Biol. **58**, 6065 (2013).
[6] G. Vasilakis, J. M. Brown, T. W. Kornack, and M. V. Romalis, Phys. Rev. Lett. **103**, 261801 (2009).
[7] I. Altarev *et al.*, Phys. Rev. Lett. **103**, 081602 (2009).
[8] M. P. Ledbetter, I. M. Savukov, V. M. Acosta, D. Budker, and M. V. Romalis, Phys. Rev. A **77**, 033408 (2008).
[9] W. C. Griffith, S. Knappe, and J. Kitching, Opt. Express **18**, 27167 (2010).
[10] S. J. Smullin, I. M. Savukov, G. Vasilakis, R. K. Ghosh, and M. V. Romalis, Phys. Rev. A **80**, 033420 (2009).
[11] R. E. Slocum and F. N. Reilly, IEEE Trans. Nucl. Sci. **10**, 165 (1963).
[12] S. J. Seltzer and M. V. Romalis, Appl. Phys. Lett. **85**, 4804 (2004).
[13] H. Dong, H. Lin, and X. Tang, IEEE Sens. J. **13**, 186 (2013).
[14] A. L. Bloom, Appl. Opt. **1**, 61 (1962).
[15] A. J. Fairweather and M. J. Usher, J. Phys. E **5**, 986 (1972).
[16] A. K. Vershovskii, Tech. Phys. Lett. **37**, 140 (2011).
[17] H. Lee, M. Fleischhauer, and M. O. Scully, Phys. Rev. A **58**, 2587 (1998).
[18] K. Cox, V. I. Yudin, A. V. Taichenachev, I. Novikova, and E. E. Mikhailov, Phys. Rev. A **83**, 015801 (2011).
[19] S. Pustelny, W. Gawlik, S. M. Rochester, D. F. J. Kimball, V. V. Yashchuk, and D. Budker, Phys. Rev. A **74**, 063420 (2006).
[20] W. E. Bell and A. L. Bloom, Phys. Rev. Lett. **6**, 280 (1961).
[21] W. Gawlik, L. Krzemień, S. Pustelny, D. Sangla, J. Zachorowski, M. Graf, A. O. Sushkov, and D. Budker, Appl. Phys. Lett. **88**, 131108 (2006).
[22] J. M. Higbie, E. Corsini, and D. Budker, Rev. Sci. Instrum. **77**, 113106 (2006).
[23] J. Rasson, Geophys. Trans. (Budapest) **36**, 187 (1991).
[24] O. Gravrand, A. Khokhlov, J. L. L. Mouël, and J. M. Léger, Earth Planets Space **53**, 949 (2001).
[25] A. Vershovskii, M. Balabas, A. Ivanov, V. Kulyasov, A. Pazgalev, and E. Aleksandrov, Tech. Phys. **51**, 112 (2006).
[26] B. Patton, O. O. Versolato, D. C. Hovde, E. Corsini, J. M. Higbie, and D. Budker, Appl. Phys. Lett. **101**, 083502 (2012).
[27] J. M. Higbie, S. M. Rochester, B. Patton, R. Holzlöhner, D. Bonaccini Calia, and D. Budker, Proc. Natl. Acad. Sci. U.S.A. **108**, 3522 (2011).
[28] C. A. Baker, D. D. Doyle, P. Geltenbort, K. Green, M. G. D. van der Grinten, P. G. Harris, P. Iaydjiev, S. N. Ivanov, D. J. R. May, J. M. Pendlebury, J. D. Richardson, D. Shiers, and K. F. Smith, Phys. Rev. Lett. **97**, 131801 (2006).
[29] P. Knowles, G. Bison, N. Castagna, A. Hofer, A. Mtchedlishvili, A. Pazgalev, and A. Weis, Nucl. Instrum. Methods Phys. Res., Sect. A **611**, 306 (2009).
[30] I. Altarev, D. Beck, S. Chesnevskaya, T. Chupp, W. Feldmeier, P. Fierlinger, A. Frei, E. Gutsmiedl, F. Kuchler, P. Link, T. Lins, M. Marino, J. McAndrew, S. Paul, G. Petzoldt, A. Pichlmaier, R. Stoepler, S. Stuiber, and B. Taubenheim, Nuovo Cimento Soc. Ital. Fis. **35C**, 122 (2012).
[31] B. Patton, D. C. Hovde, J. McAndrew, M. Sturm, P. Fierlinger, A. Schnabel, S. Sharma, D. Beck, M. Balabas, and D. Budker (to be published).
[32] See the Supplemental Material at http://link.aps.org/supplemental/10.1103/PhysRevLett.113.013001 for a discussion of the difference between the shifts induced by a light-shift beam and a magnetic field.
[33] B. S. Mathur, H. Tang, and W. Happer, Phys. Rev. **171**, 11 (1968).
[34] C. Cohen-Tannoudji and J. Dupont-Roc, Phys. Rev. A **5**, 968 (1972).
[35] T. Moriyasu, D. Nomoto, Y. Koyama, Y. Fukuda, and T. Kohmoto, Phys. Rev. Lett. **103**, 213602 (2009).
[36] S. J. Seltzer *et al.*, J. Chem. Phys. **133**, 144703 (2010).
[37] V. V. Yashchuk, D. Budker, and J. R. Davis, Rev. Sci. Instrum. **71**, 341 (2000).
[38] D. Budker, W. Gawlik, D. F. Kimball, S. M. Rochester, V. V. Yashchuk, and A. Weis, Rev. Mod. Phys. **74**, 1153 (2002).
[39] Unlike conventional polarization-maintaining fiber, the HB830Z transmits only light which is linearly polarized along one of the axes of the anisotropic fiber core; the other polarization experiences large attenuation.
[40] P. Kwee, B. Willke, and K. Danzmann, Appl. Phys. B **102**, 515 (2011).
[41] V. Acosta, M. P. Ledbetter, S. M. Rochester, D. Budker, D. F. J. Kimball, D. C. Hovde, W. Gawlik, S. Pustelny, J. Zachorowski, and V. V. Yashchuk, Phys. Rev. A **73**, 053404 (2006).
[42] R. Jiménez-Martínez, S. Knappe, and J. Kitching, Rev. Sci. Instrum. **85**, 045124 (2014).